

# The Three-Body Structure of $2n$ and $2p$ Halo Nuclei

I. SREEJA AND M. BALASUBRAMANIAM

Department of Physics, Bharathiar University, Coimbatore-641046, India.

**Email:** [m.balou@gmail.com](mailto:m.balou@gmail.com)

Received: November 17, 2017 | Revised: December 27, 2017 | Accepted: January 05, 2018

Published online: February 05, 2018

The Author(s) 2018. This article is published with open access at [www.chitkara.edu.in/publications](http://www.chitkara.edu.in/publications)

**Abstract** A three-cluster model developed for ternary fission studies has been applied for the first time to study the three-body structure of  $2n$  and  $2p$  halo nuclei. For the experimentally known  $2n$ ,  $2p$  halo nuclei, all possible ternary fragmentation potential energy surface (PES) is calculated. The two-body breakup reported earlier, clearly indicated a strong minimum in the PES corresponding to  $1n/1p$  and/or  $2n/2p$  cluster plus core configuration. However, the present calculations of PES reveal that, the three-body breakup does not result always with  $2n$  and/or  $2p$  as a cluster. A  $1n$  and/or  $1p$  cluster along with the core is initially formed, and then the core loses one nucleon to make either a  $2n$  plus core or  $2p$  plus core structure. The results are substantiated with the calculations of preformation probability calculated within quantum mechanical fragmentation theory.

**Keywords:** Halo nuclei, Cluster Core model, Preformation Probability

## 1. INTRODUCTION

The term ‘halo’ is familiar to all of us and is used in wide areas with different meanings. In nuclear physics, a halo nucleus means, the nucleus with a large spatial extension caused by protons or neutrons around the central core. The idea about the nuclear halo structure first came into focus through the experiments done by Tanihata *et al.* In an experiment made at Lawrence Berkeley Laboratory to measure the interaction cross sections and nuclear radii of various nuclei, they identified the  $^{11}\text{Li}$  nucleus with a large radius and deformation. These nuclei with larger radius are termed as “Halo” nuclei and are found to exist at the extreme edges of the table of nuclides-*viz.*, the neutron and proton drip-line. They are characterized by a very small separation energy, and very short half-lives (milliseconds). The separation energy of the outer nucleons is really small and nuclear halo appears once when it has small binding energy and low angular momentum. Two-body halos occur for nucleons in *s*- or *p*- states. Three-body halos form with hyper-spherical quantum numbers  $K = 0$  or  $K = 1$ .

Journal of Nuclear  
Physics, Material  
Sciences, Radiation and  
Applications  
Vol-5, No-2,  
February 2018  
pp. 265–281

After the experimental reports of Tanihata et al., [1-3] several studies of neutron/proton halos are done both experimentally and theoretically. Direct mass measurement of the two-neutron halo nucleus  ${}^6\text{He}$  and improved mass measurement for the four-neutron halo  ${}^8\text{He}$  are done using the TITAN Penning trap mass spectrometer at the ISAC facility which helps for the precise test of three-body forces at neutron-rich extremes [4]. Danilin et al. [5] studied the halo structure of the three-body Borromean continuum theory using the method of hyper-harmonics with core + n + n. Gupta et al. [6-9] studied the halo structure of neutron and proton drip line nuclei for both  $1n/2n$  and  $1p/2p$  using the cluster - core model. They reported that the stability of the core nucleus is found to be at both  $N=2Z$  and  $2Z \pm 2$ . Three-body halo structure of  ${}^{22}\text{C}$  ( ${}^{20}\text{C} + n + n$ ) is studied by Horoiuchi et al. [10] using the orthogonality constraint. Similar studies are carried out for  ${}^{11}\text{Li}$  and  ${}^{14}\text{Be}$  using zero-range interactions [11]. Two neutron halo structure of  ${}^{20}\text{C}$  is studied using three-body formalism, which showed the occurrence of at least two Efimov states [12]. Using the microscopic self-consistent relativistic mean field description, Shi-Sheing Zhang et al., predicted a p-orbit  $1n$  halo structure for  ${}^{31}\text{Ne}$  and found that there is no evidence of an s-orbit  $1n$  halo in  ${}^{29}\text{Ne}$  [13]. The halo structure of Borromean systems like  ${}^{11}\text{Li}$ ,  ${}^{14}\text{Be}$  and  ${}^{22}\text{C}$  are studied by Souza et al. [14]. Two neutron halo structure of  ${}^{22}\text{C}$  is studied using a Glauber model [15]. Recently an effective field theory has been used to study the three-body halo structure of  ${}^6\text{He}$  [16].

In Ref. [17,18], the concept of low proton separation energy and abnormal occupation of outside protons is used for the studies of proton halos. Using the nonlinear RMF theory Ren et al. [19] studied the halo structure of  ${}^{26}\text{P}$  ( $1p$  halo) and  ${}^{27}\text{S}$  ( $2p$  halo). The first experimental measurement of  $2p$  removal was done by Kanungo et al. [20,21] using  ${}^{17}\text{Ne}$ . Grigorenko et al. [22] studied the possibility of two-proton halo in  ${}^{17}\text{Ne}$  using three-body models. Geithner et al. [23] experimentally measured the charge radii of  ${}^{18-23}\text{Ne}$  for the first time and figured out the  $2p$  halo structure of  ${}^{17}\text{Ne}$  using Penning trap mass spectrometry and collinear laser spectroscopy. A recent study [24] of the  $2p$  halo structure of  ${}^{17}\text{Ne}$  using MCM disagrees with the previous results.

In the present work, encouraged by the success of cluster-core model, in the a priori prediction of halo nuclei, we extended the ideas of CCM into the three-cluster model proposed by one of us for the studies of ternary fission. Within three-cluster model, the three-body breakup of all the known  $2n/2p$  halo nuclei are studied. Further, the charge minimized ternary fragmentation potential of halo nuclei is used to calculate the preformation probability for the first time within quantum mechanical fragmentation theory. In section 2, a brief account on the cluster-core model, and three-cluster model is discussed.

In section 3, the obtained results are presented and discussed. Finally, in section 4, the summary and conclusions are outlined.

## 2. METHOD

The cluster-core model (CCM), of Gupta and collaborators [6-9] is an extension of preformed cluster-core model [25-29]. Earlier using CCM, the two body fragmentation potential energy surfaces (PES) of known halo nuclei were studied. Taking clue from CCM, for the first time, we extended the study to the three-body fragmentation using the three-cluster model (TCM) [30-37].

### 2.1 The cluster-core model (CCM)

In CCM, the binary fragmentation potential between the two fragments is calculated as

$$V_{tot} = \sum_{i=1}^2 m_x^i + V_C + V_p \quad (1)$$

Here  $m_x^i$  are the mass excesses of the fragments in energy units taken from Audi-Wapstra [38] and Moller-Nix [39] tables. For neutron clusters, the mass excess is taken as  $x\Delta m_n$ , where  $x$  is the number of neutrons and  $\Delta m_n = 8.0713 \text{ MeV}$ . For proton clusters, it is taken as  $x\Delta m_p - a_c A_2^{\frac{5}{3}}$ , where  $x$  is the number of protons and  $\Delta m_p = 7.2880 \text{ MeV}$  and  $a_c = 0.7053 \text{ MeV}$ .

$$V_C = \frac{Z_1 Z_2 e^2}{R_i} \quad (2)$$

is the Coulomb interaction energy between the two fragments, where  $R_i = R_1 + R_2$  is the radius of the fragments in the touching configuration, which is defined as  $R_i = 1.28 A_i^{2/3} - 0.76 + 0.8 A_i^{-1/3} \text{ fm}$  ( $i$  - is taking the values of 1 and 2 for the two-body fragmentation).

According to Blocki et al. [40] the proximity potential  $V_p$  is,

$$V_p = 4\pi \bar{R} \gamma b \Phi(\xi). \quad (3)$$

Here the mean curvature radius,  $\bar{R}$  has the form,

Sreeja, I  
Balasubramaniam, M

$$\bar{R} = \frac{R_1 R_2}{R_1 + R_2} \quad (4)$$

The specific nuclear surface tension  $\gamma$  is given by

$$\gamma = 0.9517 \left[ 1 - 1.7826 \left( \frac{N-Z}{A} \right)^2 \right] \text{MeV fm}^2 \quad (5)$$

Here  $N$ ,  $Z$  and  $A$  are the neutron, charge and mass number of the parent nucleus.  $b$  is the diffuseness of the nuclear surface given by

$$b = \left[ \pi / 2\sqrt{3} \ln 9 \right]_{t_{10-90}} \quad (6)$$

Here  $t_{10-90}$  is the thickness of the surface in which the density profile changes from 90% to 10%. The value of  $b = 0.99$  fm.

$$\Phi(\xi) = \begin{cases} -\frac{1}{2}(\xi - 2.54)^2 - 0.0852(\xi - 2.54)^3 & \text{for } \xi \leq 1.2511 \\ -3.437 \exp\left(-\frac{\xi}{0.75}\right) & \text{for } \xi \geq 1.2511 \end{cases} \quad (7)$$

Where,  $\xi = \frac{s}{b}$ . Here this function is zero as separation distance  $s(R_{12} - R_1 - R_2) = 0$  for touching configuration.

The cluster preformation probability  $P_0$  is obtained by solving the Schrödinger equation in  $\eta$  motion at fixed  $R$ ,

$$\left[ -\frac{\hbar^2}{2\sqrt{B_{\eta}}} \frac{\partial}{\partial \eta} \frac{1}{\sqrt{B_{\eta}}} \frac{\partial}{\partial \eta} + V(\eta) \right] \psi''(\eta) = E_{\eta}'' \psi''(\eta) \quad (8)$$

Solving this equation numerically,  $|\psi(\eta)|^2$  gives the probability of finding the mass fragmentation  $\eta$  at a fixed position  $R$  on the decay path. Normalizing and scaling  $|\psi(\eta)|^2$  to give the fractional mass yield at, say, the mass  $A_2$  of the cluster  $\left( d\eta = \frac{2}{A} \right)$ , the cluster preformation probability, for the ground state decay, in this model is

$$P_0(A_i) = |\psi(\eta(A_i))|^2 \sqrt{B_{\eta}(\eta)} \left(\frac{2}{A}\right) \quad (9)$$

$B_{\eta}(\eta)$  is the mass parameter which represents the kinetic energy part in the above equations are the smooth hydrodynamical mass parameters of Kröger and Scheid [41]. This gives a simple analytical expression which is found to compare nicely with microscopic cranking model calculations.

For the  $B_{\eta}$  mass we get,

$$B_{\eta} = \frac{AmR^2}{4} \left[ \frac{\nu_t(1+\beta)}{\nu_c(1+\delta^2)-1} \right] \quad (10)$$

with

$$\beta = \frac{R_c}{2R} \left[ \frac{1}{1+\cos\theta_1} \left(1 - \frac{R_c}{R_1}\right) + \frac{1}{1+\cos\theta_2} \left(1 - \frac{R_c}{R_2}\right) \right] \quad (11)$$

$$\delta = \frac{1}{2R} \left[ (1-\cos\theta_1)(R_1 - R_c) + (1-\cos\theta_2)(R_2 - R_c) \right] \quad (12)$$

$$\nu_c = \pi R_c^2 R \quad (13)$$

and  $\nu_t = \nu_1 + \nu_2$ , is the total conserved volume.

The angles  $\theta_1 = \theta_2 = 0$  and  $\delta = 0$ , correspond to two touching spheres.  $R_c (\neq 0)$  is the radius of a cylinder of length  $R$ , having a homogeneous flow in it, whose existence is assumed for the mass transfer between the two spherical nuclei (The flow in nuclei is assumed to be radial). The authors use a special Ansatz for  $R_c$ :

$$R_c = a \cdot \min(R_1, R_2) \cdot f\left(\frac{R}{R_i}\right) \quad (14)$$

with  $f(x) = 1$  for  $x \leq 1$  and  $a = 0.4$  to  $0.8$  for the best fit to the microscopic calculations.

## 2.2 The three-cluster model

Three-body fragmentation potential of all possible combinations is calculated using the TCM by imposing the condition  $A_1 \geq A_2 \geq A_3$  on the masses to avoid repetition of the combinations. The potential is calculated using

$$V_{tot} = \sum_{i=1}^3 m_x^i + \sum_{i=1}^3 \sum_{j=i}^3 V_{ij} \quad (15)$$

---

where

$$V_{ij} = V_{Cij} + V_{Pij} \quad (16)$$

Here, for the Coulomb interaction energy,  $V_{Cij} = \frac{Z_1 Z_2 e^2}{R_{ij}}$ , the radius between the fragments  $R_{ij}$  is taken as,

$$\begin{aligned} R_{12} &= R_1 + R_2 \\ R_{23} &= R_2 + R_3 \end{aligned}$$

and

$$R_{31} = R_3 + 2R_2 + R_1.$$

And for the proximity potential,  $V_{Pij} = 4\pi \bar{R}_{ij} \gamma b \Phi(\xi)$ ,  $\bar{R}_{ij}$  has the form,

$$\begin{aligned} \bar{R}_{12} &= \frac{R_1 R_2}{R_1 + R_2} \\ \bar{R}_{23} &= \frac{R_2 R_3}{R_2 + R_3} \end{aligned}$$

and

$$\bar{R}_{31} = \frac{R_3 R_1}{R_3 + 2R_2 + R_1}$$

In the specific nuclear surface tension  $\gamma$ , the terms  $N$ ,  $Z$  and  $A$  changes for each two fragments.

---

$$\begin{aligned} A_{ij} &= A_i + A_j \\ Z_{ij} &= Z_i + Z_j \end{aligned}$$

and

$$N_{ij} = A_{ij} - Z_{ij}$$

The universal function  $\Phi(\xi)$  depends only on the surface separation  $s = R_{ij} - (R_i + R_j)$ . It is negative in the overlap region, zero in the touching configuration and is positive in the separated configuration. In this model, the potential energies are calculated for all possible cluster-core  $(A_2 - A_1) \& ([A_3, A_2] - A_1)$  configurations which help to find the neutron(s) or proton(s) cluster + core configuration with a minimum potential energy.

### 3. RESULTS

We have investigated the three-body structure of 1n, 1p, 2n and 2p halo nuclei within the three-cluster model. The three-body potential energy surfaces (PES) calculated for all the proton-rich and neutron-rich halo nuclei are shown in table 1. The first column of the table lists the parent halo nucleus. The second to fourth column lists the deepest minimum in the PES for each nucleus along with any other pronounced minimum of the cluster 1, cluster 2 and the core nucleus resulting from the potential energy calculations. In column 5 and 6, the Z and N values of the core is presented. When the PES was calculated for a two-body breakup as was reported in [5,6], the PES clearly indicated a stronger preference for the halo cluster plus core configuration. The halo configuration corresponding to two body potential is listed in the last column of the table.

If we consider the three-body breakup and in turn the three-body fragmentation potential, the scenario is not as it was before. For example, a 2n-halo like  ${}^6\text{He}$  exhibits, stronger minima corresponding to either  $1n + {}^2\text{H} + {}^3\text{H}$  or  ${}^1n + {}^1\text{H} + {}^4\text{H}$ . This indicates, that, it forms as a breakup with 1n as one of the clusters and then 1n from either  ${}^3\text{H}$  or  ${}^4\text{H}$  gives rise to a 2n cluster and the remaining  ${}^2\text{H} + {}^2\text{H}$  in the former case and  ${}^1\text{H} + {}^3\text{H}$  in the later case forms as  ${}^4\text{He}$ , finally giving rise to a  $2n + {}^4\text{He}$  structure. We interpret that, 2n or 2p halo nuclei are first formed as a three-body structure with 1n or 1p cluster and then would finally result in the amalgamation of remaining two clusters to form a core donating 1n and/or 1p to result in 2n and/ or 2p cluster plus core.

Figures 1 to 4 present the three-body potential energy surface as defined in Eq. (15) as a function of the three mass numbers denoted by  $A_1, A_2$  and  $A_3$

Sreeja, I  
Balasubramaniam, M

corresponding to some representative cases of 2n halo ( $^{11}\text{Li}$  and  $^{19}\text{B}$ ), 1n halo ( $^{14}\text{B}$  and  $^{24}\text{F}$ ), 2p halo ( $^{20}\text{Mg}$  and  $^{27}\text{S}$ ), and 1p halo ( $^8\text{B}$  and  $^{26}\text{P}$ ) nuclei. In Fig.1, the three-body potential energy surface as a function of mass numbers  $A_1, A_2$  and  $A_3$  for the 2n-halo nuclei  $^{11}\text{Li}$  and  $^{19}\text{B}$  are presented in a four-dimensional ternary contour graph. For  $^{11}\text{Li}$ , a stronger minimum in the potential energy surface is seen corresponding to  $^5_1\text{H} + ^4_2\text{He} + ^2_0\text{n}$ . The three-body breakup results in 2n as one of the cluster and the remaining cluster and core will amalgamate to form  $^9_3\text{Li}$ . However, for  $^{19}\text{B}$  two pronounced minima are seen in the PES. The numerically strongest minimum corresponds to  $^{13}_3\text{Li} + ^4_2\text{He} + ^2_0\text{n}$  and the other minimum corresponds to  $^9_3\text{Li} + ^9_2\text{He} + ^1_0\text{n}$ . Since,  $^{19}\text{B}$  is an established 2n-halo, the first minimum may be the preferable path at the same time, the second possibility in which either the least stable  $^9_2\text{He}$  could lose 1n to form a 2n cluster plus core, can also be not ruled out. Similar results are presented in figures 3 to 4 for 1n, 2p and 1p halo nuclei.

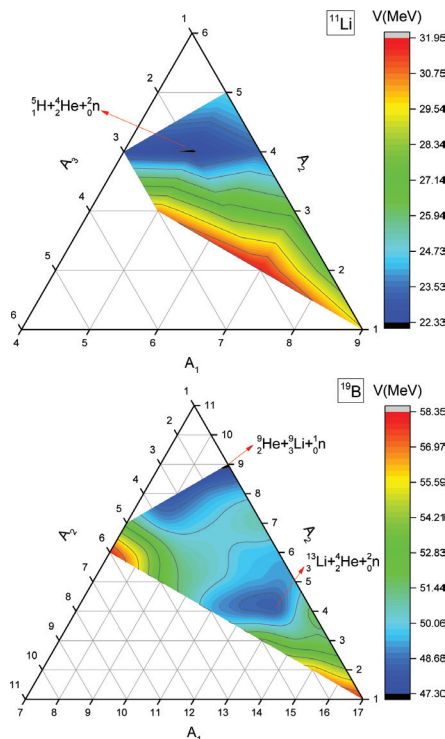


**Figure 1:** Three-body potential energy surface as a function of mass numbers  $A_1, A_2$  and  $A_3$  for the 2n-halo nuclei  $^{11}\text{Li}$  and  $^{19}\text{B}$ . Stronger minima in the potential energy surface are labelled.

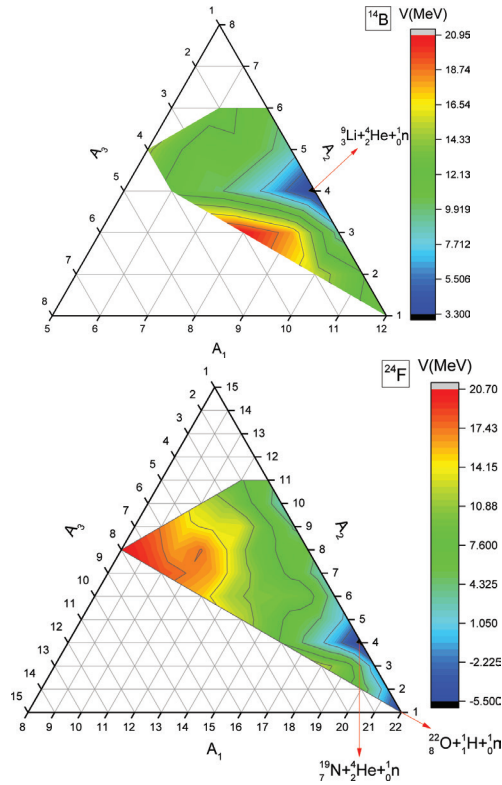


**Figure 2:** Three-body potential energy surface as a function of mass numbers  $A_1$ ,  $A_2$  and  $A_3$  for the 1n-halo nucleus  $^{14}\text{B}$ ,  $^{24}\text{F}$ . Stronger minima in the potential energy surface are labelled.

In each figure, the stronger minimum in the PES is labelled. In some cases, more than one minimum is present, indicating different possible rearrangements of the nucleons finally to observe them as either 1n/2n or 1p/2p halo nuclei. Similar calculations are done for all the nuclei studied and are listed in table 1.

To further substantiate our result, we present in Table 2, the preformation probability values calculated for some selected cases of 1n, 1p and 2n and 2p halo nuclei. The preformation probability is calculated for the two-body fragmentation potential as defined in Eq. (1). For the use of this fragmentation potential and the mass parameters defining the kinetic energy part of the Hamiltonian as defined in Eq. (10), the equation of motion given in Eq. (8) is solved. The square modulus of the wave function after normalization gives the preformation probability as denoted in Eq. (9).

It is clearly seen from the Table 2, that, 1n+core and/or 1p+core nuclei are found to have a larger probability of formation supporting the results seen

Sreeja, I  
Balasubramaniam, M

**Table 1:** The deepest minima seen in the three-body potential energy surface of the known 1n, 1p, 2n and 2p halo nuclei are listed. If there is more than one pronounced minimum in the PES, which is also listed.

Parent	Cluster1 $A_3$	Cluster2 $A_2$	Core $A_1$	Z (Core)	N (Core)	Remarks
${}^6\text{He}$	${}^1_0n$	${}^2_1H$	${}^3_1H$	1	2	2n halo
	${}^1_0n$	${}^1_1H$	${}^4_1H$	1	3	
${}^{11}\text{Be}$	${}^1_0n$	${}^4_2He$	${}^6_2He$	2	4	1n halo
	${}^2_0n$	${}^4_2He$	${}^5_2He$	2	3	
${}^{14}\text{B}$	${}^1_0n$	${}^4_2He$	${}^9_3Li$	3	6	1n halo
	${}^2_0n$	${}^4_2He$	${}^8_3Li$	3	5	
${}^{15}\text{C}$	${}^1_0n$	${}^4_2He$	${}^{10}_4Be$	4	6	1n halo
	${}^2_0n$	${}^4_2He$	${}^9_4Be$	4	5	
${}^{17}\text{B}$	${}^1_0n$	${}^4_2He$	${}^{12}_3Li$	3	9	2n halo
	${}^2_0n$	${}^4_2He$	${}^{11}_3Li$	3	8	
${}^{17}\text{C}$	${}^1_0n$	${}^4_2He$	${}^{12}_4Be$	3	9	1n halo
	${}^2_0n$	${}^4_2He$	${}^{11}_4Be$	4	7	
${}^{19}\text{B}$	${}^1_0n$	${}^9_3Li$	${}^9_2He$	2	7	2n halo
	${}^2_0n$	${}^{13}_3Li$	${}^4_2He$	2	6	
${}^{19}\text{C}$	${}^1_0n$	${}^4_2He$	${}^{14}_4Be$	4	10	1n halo
	${}^2_0n$	${}^4_2He$	${}^{13}_4Be$	4	9	
${}^{22}\text{N}$	${}^1_0n$	${}^3_1H$	${}^{18}_6C$	6	12	1n halo
	${}^1_0n$	${}^4_2He$	${}^{17}_5B$	5	12	
${}^{22}\text{O}$	${}^1_0n$	${}^4_2He$	${}^{17}_6C$	6	11	1n halo
	${}^2_0n$	${}^4_2He$	${}^{16}_6C$	6	10	

							The Three-Body Structure of 2n and 2p Halo Nuclei
$^{23}\text{N}$	$^1_0n$	$^3_1\text{H}$	$^{19}_6\text{C}$	6	13	2n halo	
	$^1_0n$	$^2_1\text{H}$	$^{20}_6\text{C}$	6	14		
$^{23}\text{O}$	$^1_0n$	$^4_2\text{He}$	$^{18}_6\text{C}$	6	12	1n halo	
	$^2_0n$	$^4_2\text{He}$	$^{17}_6\text{C}$	6	11		
$^{24}\text{F}$	$^1_0n$	$^4_2\text{He}$	$^{19}_7\text{N}$	7	12	1n halo	
	$^1_0n$	$^1_1\text{H}$	$^{22}_8\text{O}$	8	14		
$^{24}\text{O}$	$^1_0n$	$^4_2\text{He}$	$^{19}_6\text{C}$	6	13	1n halo	
	$^2_0n$	$^2_2\text{He}$	$^{18}_6\text{C}$	6	12		
$^{26}\text{F}$	$^1_0n$	$^4_2\text{He}$	$^{21}_7\text{N}$	7	14	1n halo	
	$^1_0n$	$^1_1\text{H}$	$^{24}_8\text{O}$	8	16		
$^{27}\text{F}$	$^1_0n$	$^4_2\text{He}$	$^{22}_7\text{N}$	7	15	2n halo	
	$^1_0n$	$^1_1\text{H}$	$^{24}_8\text{O}$	8	16		
$^{29}\text{Ne}$	$^1_0n$	$^4_2\text{He}$	$^{24}_8\text{O}$	8	16	1n halo	
	$^1_0n$	$^5_2\text{He}$	$^{23}_8\text{O}$	8	15		
$^{31}\text{Ne}$	$^1_0n$	$^4_2\text{He}$	$^{26}_8\text{O}$	8	18	1n halo	
	$^1_0n$	$^6_2\text{He}$	$^{24}_8\text{O}$	8	16		
$^8\text{B}$	$^1_1p$	$^3_2\text{He}$	$^4_2\text{He}$	2	2	1p halo	
	$^1_1p$	$^1_0n$	$^6_4\text{Be}$	4	2		
$^9\text{C}$	$^1_1p$	$^4_2\text{He}$	$^4_3\text{Li}$	3	1	2p halo	
	$^2_2p$	$^3_2\text{He}$	$^4_2\text{He}$	2	2		
$^{12}\text{N}$	$^1_1p$	$^4_2\text{He}$	$^7_4\text{Be}$	4	3	1p halo	
	$^3_2\text{He}$	$^4_2\text{He}$	$^5_3\text{Li}$	3	2		
$^{17}\text{F}$	$^1_1p$	$^8_4\text{Be}$	$^8_4\text{Be}$	4	4	1p halo	
	$^4_2\text{He}$	$^4_2\text{He}$	$^9_5\text{B}$	5	4		
$^{17}\text{Ne}$	$^1_1p$	$^4_2\text{He}$	$^{21}_7\text{N}$	7	5	2p halo	
	$^2_2p$	$^4_2\text{He}$	$^{11}_6\text{C}$	6	5		

Sreeja, I  
Balasubramaniam, M

$^{18}\text{Ne}$	$^1_1p$	$^4_2\text{He}$	$^{13}_7\text{N}$	7	6	2p halo
	$^4_2\text{He}$	$^4_2\text{He}$	$^{10}_6\text{C}$	6	4	
$^{26}\text{P}$	$^1_1p$	$^4_2\text{He}$	$^{21}_{12}\text{Mg}$	12	9	1p halo
	$^1_1p$	$^1_0n$	$^{24}_{14}\text{Si}$	14	10	
$^{27}\text{P}$	$^1_1p$	$^4_2\text{He}$	$^{22}_{12}\text{Mg}$	12	10	1p halo
	$^2_2p$	$^4_2\text{He}$	$^{21}_{11}\text{Na}$	11	10	
$^{27}\text{S}$	$^1_1p$	$^4_2\text{He}$	$^{22}_{13}\text{Al}$	13	9	2p halo
	$^2_2p$	$^4_2\text{He}$	$^{21}_{12}\text{Mg}$	12	9	
$^8\text{He}$	$^2_0n$	$^3_1\text{H}$	$^3_1\text{H}$	1	2	2n halo
	$^1_0n$	$^3_1\text{H}$	$^4_1\text{H}$	1	3	
$^{11}\text{Li}$	$^2_0n$	$^4_2\text{He}$	$^5_1\text{H}$	1	4	2n halo
	$^3_0n$	$^4_2\text{He}$	$^4_1\text{H}$	1	3	
$^{12}\text{Be}$	$^2_0n$	$^4_2\text{He}$	$^6_2\text{He}$	2	4	2n halo
	$^1_0n$	$^4_2\text{He}$	$^7_2\text{He}$	2	5	
$^{14}\text{Be}$	$^2_0n$	$^4_2\text{He}$	$^8_2\text{He}$	2	6	2n halo
	$^1_0n$	$^4_2\text{He}$	$^9_2\text{He}$	2	7	
$^{22}\text{C}$	$^2_0n$	$^{10}_4\text{Be}$	$^{10}_2\text{He}$	2	8	2n halo
	$^2_0n$	$^4_2\text{He}$	$^{16}_4\text{Be}$	4	12	
$^{29}\text{F}$	$^2_0n$	$^4_2\text{He}$	$^{23}_7\text{N}$	7	16	2n halo
	$^1_0n$	$^3_1\text{H}$	$^{25}_8\text{O}$	8	17	
$^{20}\text{Mg}$	$^2_2p$	$^4_2\text{He}$	$^{14}_8\text{O}$	8	6	2p halo
	$^1_1p$	$^4_2\text{He}$	$^{15}_9\text{F}$	9	6	
$^{11}\text{N}$	$^3_3p$	$^4_2\text{He}$	$^4_2\text{He}$	2	2	1p halo
	$^2_2p$	$^4_2\text{He}$	$^5_3\text{Li}$	3	2	

through PES for the two-body breakup. At the same time, for 2n and/or 2p halo nuclei, the preformation probability values are found to be very low compared to 1n and/or 1p halo nuclei results. This result reported for the first time for

**Table 2:** The preformation probability values for the use of two-body breakup potential for some representative cases of 1n, 1p, 2n and 2p halo nuclei.

The Three-Body Structure of 2n and 2p Halo Nuclei

Halo	Parent	Preformation Probability
1n – halo	$^{22}\text{N}$	0.932
1n - halo	$^{24}\text{F}$	0.978
1p -halo	$^{26}\text{P}$	0.932
1p - halo	$^{27}\text{P}$	0.990
2n-halo	$^{22}\text{C}$	0.661
2n-halo	$^{27}\text{F}$	0.626
2p-halo	$^{20}\text{Mg}$	0.668
2p-halo	$^{27}\text{S}$	0.562

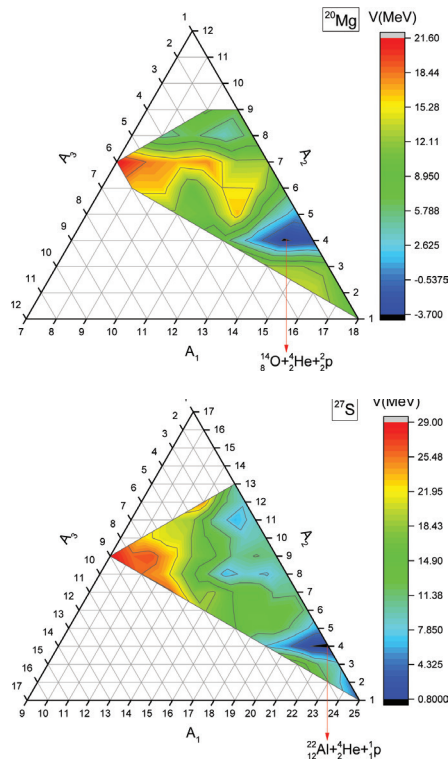


**Figure 3:** Three-body potential energy surface as a function of mass numbers  $A_1$ ,  $A_2$  and  $A_3$  for the 2p halo nuclei  $^{20}\text{Mg}$ ,  $^{27}\text{S}$ . Stronger minima in the potential energy surface are labelled.

the halo nuclei indicates, and strengthens our interpretation that, the 2n and 2p halo structure is initially formed with a larger probability as 1n plus core and/or 1p plus core and then the core nucleus, further loses either a neutron to make 2n plus the core structure or a proton to make a 2p plus core structure.

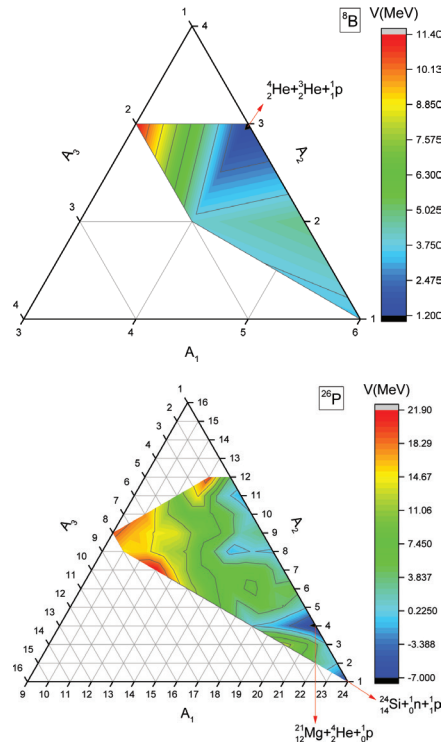


**Figure 4:** Three-body potential energy surface as a function of mass numbers  $A_1$ ,  $A_2$  and  $A_3$  for the 1p halo nuclei  $^8\text{B}$  and  $^{26}\text{P}$ . Stronger minima in the potential energy surface are labelled.

## SUMMARY AND CONCLUSIONS

Three-body breakup and the corresponding three-body fragmentation energy is calculated for investigating three-body structure of 2n and 2p halo nuclei. Unlike two-body fragmentation, which revealed clearly the core plus neutron and/or proton cluster, three-body PES exhibits more than one stronger minimum. Further the 2n / 2p three-body breakup does not always result in one of the cluster as 2n or 2p. In most of the cases, 1n or 1p cluster is preferred in the ternary breakup and hence the remaining cluster and the core nuclei must lose

a neutron and/or proton to make it as a 2n / 2p halo nuclei. This observation is interpreted as follows: the three-body structure of the 2n or 2p halo are initially forming as a three-body structure with 1n or 1p as one of the cluster, which finally results in the amalgamation of the remaining nuclei to form a core by donating either 1n and/or 1p to result in as 2n and/or 2p cluster plus core. The calculations of preformation probability also, substantiates our interpretation.

## ACKNOWLEDGEMENT

One of the authors I. Sreeja, acknowledges the financial support in the form of University Research Fellowship awarded by Bharathiar University, Coimbatore-641046.

## REFERENCES

- [1] I. Tanihata, H. Hamagaki, O. Hashimoto, S. Nagamiya et al., Phys. Lett. **160B**, 380 (1985).
- [2] I. Tanihata, H. Hamagaki, O. Hashimoto, Y. Shida et al., Phys. Rev. Lett. **55**, 2676 (1985). <https://doi.org/10.1103/PhysRevLett.55.2676>
- [3] I. Tanihata, T. Kobayashi, O. Yamakawa, S. Shimoura et al., Phys. Lett. B **206**, 592 (1988).
- [4] M. Brodeur, T. Brunner, C. Champagne, S. Effenenauer et al., Phys. Rev. Lett. **108**, 052504 (2012). <https://doi.org/10.1103/PhysRevLett.108.052504>
- [5] B. V. Danilin, I. J. Thompson, J. S. Vaagen and M. V. Zhukov, Nucl. Phys. A **632**, 383 (1998). [https://doi.org/10.1016/S0375-9474\(98\)00002-5](https://doi.org/10.1016/S0375-9474(98)00002-5)
- [6] R. K. Gupta, M. Balasubramaniam, R. K. Puri and W. Scheid, J. Phys. G: Nucl. Part. Phys. **26**, L23 (2000). <https://doi.org/10.1088/0954-3899/26/2/102>
- [7] R. K. Gupta, M. Balasubramaniam et al., J. Phys. G: Nucl. Part. Phys. **32**, 565 (2006). <https://doi.org/10.1088/0954-3899/32/4/012>
- [8] G. Sawhney, M. K. Sharma and R. K. Gupta J. Phys. G: Nucl. Part. Phys **41**, 055101 (2014). <https://doi.org/10.1088/0954-3899/41/5/055101>
- [9] R. K. Gupta, Sushil Kumar et al., J. Phys. G: Nucl. Part. Phys. **28**, 699 (2002). <https://doi.org/10.1088/0954-3899/28/4/309>
- [10] W. Horiuchi and Y. Suzuki, Phys. Rev. C **74**, 034311 (1961). <https://doi.org/10.1103/PhysRevC.74.034311>
- [11] T. Frederico, M. T. Yamashita and Lauro Tomio, Nucl. Phys. A **787**, 561c-568c (2007). <https://doi.org/10.1016/j.nuclphysa.2006.12.085>
- [12] I. Mazhumdar, Pramana - J. Phys., **75**, 81 (2010). <https://doi.org/10.1007/s12043-010-0067-y>
- [13] Shi-Sheng Zhang, M. S. Smith, Zhong-Shu Kang and Jie Zhao, Phys. Lett. B **730**, 30 (2014).

- 
- Sreeja, I  
Balasubramaniam, M
- [14] L. A. Souza, F. F. Bellotti and T. Frederico, *J. Phys.* **630**, 012043 (2015).
- [15] Y. Togano, T. Nakamura, Y. Kondo, J. A. Tostevin et al., *Phys. Lett. B* **761**, 412 (2016). <https://doi.org/10.1016/j.physletb.2016.08.062>
- [16] E. Rydberg, C. Forssen and L. Platter, *Few Body Syst.* **58**, 143 (2017).  
<https://doi.org/10.1007/s00601-017-1307-1>
- [17] W. Schwab et al., *Z. Phys. A* **350**, 283 (1995).  
<https://doi.org/10.1007/BF01291183>
- [18] A. Ozawa et al., *Phys. Lett. B* **334**, 18 (1994).  
[https://doi.org/10.1016/0370-2693\(94\)90585-1](https://doi.org/10.1016/0370-2693(94)90585-1)
- [19] Z. Ren, B. Chen, Z. Ma and G. Xu, *Phys. Rev. C* **53**, 572 (1996).  
<https://doi.org/10.1103/PhysRevC.53.R572>
- [20] R. Kanungo, M. Chiba, S. Adhikari, D. Fang et al., *Phys. Lett. B* **571**, 21 (2003).  
<https://doi.org/10.1016/j.physletb.2003.07.050>
- [21] R. Kanungo, *Nucl. Phys. A* **738**, 293 (2004).  
<https://doi.org/10.1016/j.nuclphysa.2004.04.048>
- [22] L. V. Grigorenko, Yu. L. Parfenova and M. V. Zhukov, *Phys. Rev. C* **71**, 051604(R) (2005).
- [23] W. Geithner, T. Neff, G. Audi, K. Blaum et al., *Phys. Rev. Lett.* **101**, 252502 (2008). <https://doi.org/10.1103/PhysRevLett.101.252502>
- [24] W.S. Hwash, *Int. J. Mod. Phys. E* **25**, 1650105 (2016).  
<https://doi.org/10.1142/S0218301316501056>
- [25] R. K. Gupta, *Proceedings of the Vth International Conference on Nuclear Reaction Mechanisms, Varenna, Italy (1988)* p. 416.
- [26] S. S. Malik and R. K. Gupta, *Phys. Rev. C* **39** 1992 (1989).  
<https://doi.org/10.1103/PhysRevC.39.1992>
- [27] R. K. Gupta, W. Scheid, and W. Greiner, *J. Phys. G: Nucl. Phys.* **17** 1731(1991).  
<https://doi.org/10.1088/0954-3899/17/11/018>
- [28] S. Kumar and R. K. Gupta, *Phys. Rev. C* **55** 218 (1997).  
<https://doi.org/10.1103/PhysRevC.55.218>
- [29] R. K. Gupta, in *Heavy Elements and Related New Phenomena*, edited by W. Greiner and R.K. Gupta (World Scientific, Singapore, 1999), **Vol. II**, p. 730.  
[https://doi.org/10.1142/9789812816634\\_0020](https://doi.org/10.1142/9789812816634_0020)
- [30] K. Manimaran and M. Balasubramaniam, *Phys. Rev. C* **79**, 024610 (2009).  
<https://doi.org/10.1103/PhysRevC.79.024610>
- [31] K. Manimaran and M. Balasubramaniam, *Eur. Phys. J. A* **45**, 293 (2010).  
<https://doi.org/10.1140/epja/i2010-11000-7>
- [32] K. Manimaran and M. Balasubramaniam, *J. Phys. G: Nucl. Part. Phys.* **37**, 045104 (2010). <https://doi.org/10.1088/0954-3899/37/4/045104>
-

- 
- [33] K. Manimaran and M. Balasubramaniam, Phys. Rev. C **83**, 034609 (2011).  
<https://doi.org/10.1103/PhysRevC.83.034609>
- [34] K. R. Vijayaraghavan, W. von Oertzen and M. Balasubramaniam, Eur. Phys. J. A **48**, 27 (2012). <https://doi.org/10.1140/epja/i2012-12027-4>
- [35] K. R. Vijayaraghavan, M. Balasubramaniam and W. von Oertzen, Phys. Rev. C **90**, 024601 (2014). <https://doi.org/10.1103/PhysRevC.90.024601>
- [36] M. Balasubramaniam, K. R. Vijayaraghavan and C. Karthickraj, Pramana - J. Phys., **85**, 423 (2015).
- [37] M. Balasubramaniam, K. R. Vijayaraghavan and K. Manimaran, Phys. Rev. C **93**, 014601 (2016). <https://doi.org/10.1103/PhysRevC.93.014601>
- [38] G. Audi, F. G. Kondev, M. Wang, B. Pfeiffer, X. Sun, J. Blachot and M. MacCormik, Chin. Phys. C **36(12)**, 1157 (2012)  
<https://doi.org/10.1088/1674-1137/36/12/>
- [39] P. Miller, J. R. Nix, W. D. Myers, W. J. Swiatecki, At. Data Nucl. Data Tables **59**, 185 (1995)
- [40] J. Blocki, J. Randrup, W. J. Swiatecki and C. F. Tsang, Ann. Phys. (NY) **105**, 427 (1977). [https://doi.org/10.1016/0003-4916\(77\)90249-4](https://doi.org/10.1016/0003-4916(77)90249-4)
- [41] H. Kröger and W. Scheid, J. Phys. G **6**, L85 (1980).  
<https://doi.org/10.1088/0305-4616/6/4/006>

The Three-Body  
Structure of  $2n$  and  
 $2p$  Halo Nuclei

---